Terrain Correction for Increasing the Evapotranspiration Estimation Accuracy in a Mountainous Watershed

Yi-Chen Wang, Tzu-Yin Chang, and Yuei-An Liou, *Senior Member, IEEE*

***Abstract*—Evapotranspiration (ET) plays a major role in the energy and water balances of the hydrological cycle. Monitoring ET at a regional level has become feasible with the advance of remote-sensing technology. This letter presents a module that incorporates satellite images, surface meteorological data, and topographic information in estimating ET over a tropical montane watershed. The satellite images used include Thematic Mapper (TM), Landsat-7 Enhanced Thematic Mapper Plus, and Advanced Spaceborne Thermal Emission and Reflection Radiometer with visible, near infrared, shortwave infrared, and thermal infrared bands. The estimated surface energy fluxes are compared with the *in situ* measurements. The results demonstrate that, compared to other model estimations, the proposed module with terrain correction provides the highest correlation ($r = 0.75$) between the estimated latent heat flux associated with ET and its corresponding *in situ* measurement. The proposed module will be further refined and applied to monitor long-term ET over mountainous watersheds.**

***Index Terms*—Advanced Spaceborne Thermal Emission and Reflection Radiometer (ASTER), digital elevation model (DEM), evapotranspiration (ET), Landsat, surface heat flux.**

I. Introduction

EVAPOTRANSPIRATION (ET) is an important factor affecting local and regional water exchanges in the hydrological cycle. In semiarid areas, for example, recorded pan evaporation may be nearly equal to precipitation, and regional ET is more than half of the total precipitation [1]. ET is traditionally estimated using empirical equations or model simulations with meteorological data, resulting in mostly point values for local areas. Estimating ET at a regional level, however, requires incorporating heterogeneous surface conditions [2]. This is particularly challenging when applied to tropical montane environments where vegetation diversity is high and topography is complex. Although recent advances in remote-sensing technology have enabled the estimation of spatially distributed ET [3], [4], the use of remotely sensed data in conjunction with empirical algorithms at a regional level is still restricted by topographic heterogeneity, weather conditions (particularly cloud cover), and variable land use/cover types. Most studies have thus focused on agricultural areas over flat terrain [5], [6].

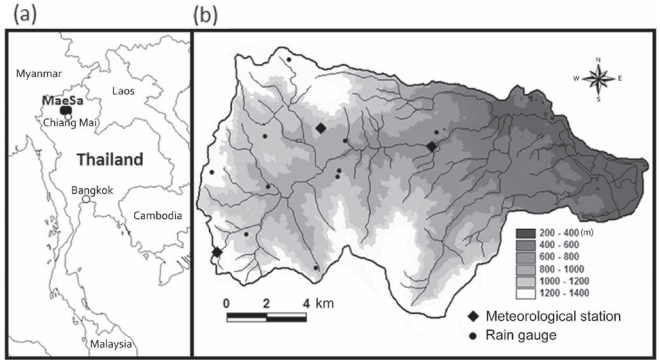

Fig. 1. (a) Location of the Mae Sa watershed. (b) Distribution of the micrometeorological and rain gauge stations in Mae Sa.

There is an urgent need to understand the regional ET in the tropical montane watersheds because the environment is undergoing dramatic landscape modification [7], thereby influencing water and energy fluxes that may have important consequences for water supply and ecosystem productivity. In this letter, we develop a Terrain-corrected Surface Energy Balance Mountain (TSEBM) module, incorporating remotely sensed images and auxiliary surface meteorological and terrain data to improve the accuracy of ET estimation in mountainous watersheds.

II. Study Site and Data

The 138 km^2 Mae Sa watershed (18.83° N to 18.94° N and 98.78° E to 98.97° E) is located in Chiang Mai Province, Thailand [Fig. 1(a)]. The topography of the watershed is mostly hilly, except for some flat plains in the eastern part. Elevation ranges from 314 to 1384 m. The watershed is characterized by a tropical monsoon climate with a rainy season that extends from late May to November. Annual mean rainfall is 1300 mm and annual mean temperature is 21.3 °C (2002–2004) [8]. The major land cover types are approximately 71% forest and 25% agriculture. Three micrometeorological stations and a network of gauges measuring precipitation and/or soil moisture have been established in the watershed since 2004 [Fig. 1(b)], recording surface meteorological and hydrological data at a 20-min interval.

Data used in this letter include *in situ* measurements, satellite images, and digital elevation model (DEM). The *in situ* measurements are the surface energy fluxes obtained from the three

Manuscript received May 29, 2009; revised July 31, 2009. Date of publication November 24, 2009; date of current version April 14, 2010. The works of Y.-C. Wang and T.-Y. Chang were supported by the National University of Singapore (NUS) under Grant R-109-000-070-101.

Y.-C. Wang and T.-Y. Chang are with the Department of Geography, National University of Singapore, Singapore 117570 (e-mail: geowyc@nus.edu.sg; geoct@nus.edu.sg; 92643007@cc.ncu.edu.tw).

Y.-A. Liou is with the Institute of Space Science and Center for Space and Remote Sensing Research, National Central University, Chung-Li 320, Taiwan (e-mail: yueian@csrsr.ncu.edu.tw).

Digital Object Identifier 10.1109/LGRS.2009.2035138

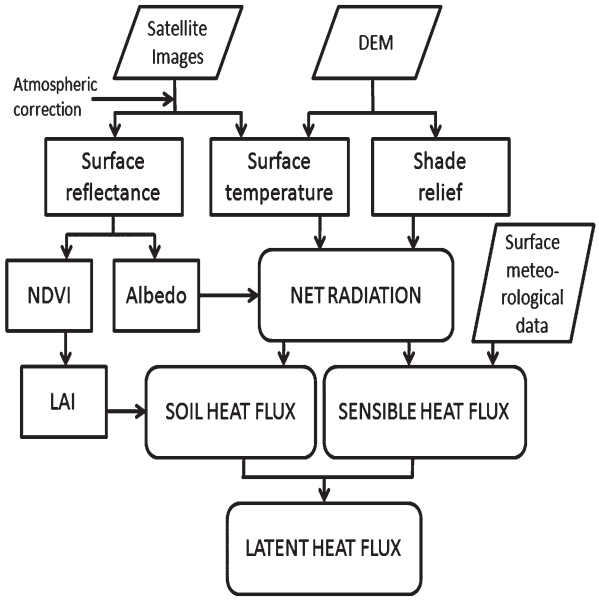

Fig. 2. Flowchart of the TSEBM module.

micrometeorological stations and are used as references in comparing with the estimations derived from satellite images. The following types of satellite images are used: Landsat-5 Thematic Mapper (TM) (acquired on February 07, 2005 Landsat-7 Enhanced TM Plus (ETM+) (April 07, 2006, January 04, 2007, January 20, 2007, April 10, 2007, and February 24, 2008), and Advanced Spaceborne Thermal Emission and Reflection Radiometer (ASTER) (February 02, 2006, and February 08, 2008) images from the Land Processes Distributed Active Archive Center, U.S. Geological Survey. Two DEMs are utilized for terrain correction. DEM_$_{\text{map}}$ is generated from digitizing contours of a 1 : 50 000 topographical map prepared by the Royal Thai Survey Department in 1994. DEM_$_{\text{ASTER}}$ is the ASTER DEM product, which is the 20080208 AST14DMO (Digital Elevation Model & Registered Radiance at the Sensor—Orthorectified) imagery. The resolutions of DEM_$_{\text{map}}$ and DEM_$_{\text{ASTER}}$ are, respectively, 20 and 30 m.

III. TSEBM Module

The method used in retrieving ET from remotely sensed data is based on basic surface energy balance theory, where ET is associated with latent heat flux. Instantaneous ET estimation (in mm/hr) is computed as

$$ET = 3600 \times (LH/\lambda) \tag{1}$$

where LH is the latent heat flux (in Wm^{-2}) and λ is the latent heat of vaporization (in kJ kg^{-1}), calculated using $2500 - 2.359 \times T_a$, with T_a as the air temperature (in °C)

The key components and the procedure of the proposed TSEBM module for LH estimation are shown in Fig. 2. The digital numbers from satellite images are first converted into spectral radiance, which is subsequently converted into surface reflectance using the fast line-of-sight atmospheric analysis of spectral hypercubes atmospheric correction module of ENVI 4.6. This process filters the interference from the path radiation, such as water vapor, aerosol, and dust particle. The surface reflectance of the visible and near-infrared (VNIR) bands and that of the shortwave infrared (SWIR) bands are then used to calculate the normalized difference vegetation index (NDVI) and surface albedo (α). Another component derived from the satellite images for net radiation calculation is surface temperature (T_0), which is converted from the thermal infrared (TIR) bands using the Planck function. These basic parameters (i.e., NDVI, surface albedo (α), and surface skin temperature (T_0)) are used in the estimation of surface heat flux.

A. Surface Energy Flux Estimation

Based on the surface energy balance theory, LH can be derived as

$$LH = R_n - G_0 - H \tag{2}$$

where R_n (in Wm^{-2}) is the net radiation at the land surface, G_0 (in Wm^{-2}) is the soil heat flux, and H (in Wm^{-2}) is the sensible heat flux. Under a stable atmospheric condition, net radiation above a canopy is the balance between incoming and outgoing radiation

$$R_n = (1-\alpha)K_s^{\downarrow} + K_L^{\downarrow} - \varepsilon_0 \sigma T_0^4 \tag{3}$$

where $K_s^{\downarrow}$ is the incoming shortwave radiation, $K_L^{\downarrow}$ is the incoming longwave radiation, α is the surface albedo, ε_0 is the surface emissivity, σ is the Stefan–Boltzmann constant $(5.67 \times 10^{-8}\ \text{Wm}^{-2}\text{K}^{-4})$, and T_0 is the surface skin temperature (in K).

Soil heat flux (G_0) is commonly estimated as a fraction of net radiation. Because the Mae Sa study area in this letter is mostly forested, the transmission of net radiation through a canopy is modified using the Beer–Bouguer law [9]. The equation is

$$G_0 = a \times R_n \exp(-b \times LAI) \tag{4}$$

where coefficients $a = 0.2$ and $b = 0.592$ are acquired, respectively, from Waters *et al.* [10] and Baldocchi *et al.* [11] and LAI denotes leaf area index, estimated as [12]

$$LAI = 0.57 \exp(2.33 \times NDVI). \tag{5}$$

The bulk transfer of sensible heat flux (H) is given by

$$H = \rho_{\text{air}} C_p dT / r_a \tag{6}$$

where ρ_{air} and C_p are, respectively, the density ($1.21\ \text{kgm}^{-3}$) and the specific heat of the air at constant pressure ($1004\ \text{J kg}^{-1}\text{K}^{-1}$), dT is the temperature difference between two heights (in K), and r_a is the aerodynamic resistance for the sensible heat (in sm^{-1}). Following Bastiaanssen *et al.* [5], a linear relationship is assumed between dT and T_0. Also, r_a is estimated using the Monin–Obukhov similarity theory [13]. Consequently, (6) can be rewritten as follows:

$$H = \frac{\kappa u^* \rho_{\text{air}} C_p dT}{\left[\ln\left(\frac{z_2 - z_d}{z_1 - z_d}\right) - \left(\Psi_h\left(\frac{z_2 - z_d}{L}\right) + \Psi_h\left(\frac{z_1 - z_d}{L}\right)\right)\right]} \tag{7}$$

$$u^* = \frac{u_b \kappa}{\ln\left(\frac{z_b}{z_{\text{om}}}\right)} \tag{8}$$

TABLE I
COMPARISON OF SURFACE ENERGY FLUXES ESTIMATED FROM FIVE MODELS WITH *IN SITU* MEASUREMENTS

Surface energy flux	Flat surface		SEBAL Mountain with DEM_map		SEBAL Mountain with DEM_ASTER		TSEBM with DEM_map		TSEBM with DEM_ASTER	
	R*	RMSE**	R	RMSE	R	RMSE	R	RMSE	R	RMSE
Net Radiation	0.67	91	0.70	200	0.70	223	0.76	98	0.78	104
Soil heat	0.36	66	0.04	82	0.08	84	0.11	40	0.10	40
Sensible heat	0.35	58	0.11	191	0.24	109	0.30	103	0.52	53
Latent heat	0.56	75	0.29	144	0.22	126	0.66	92	0.75	73

*Pearson's correlation coefficient
**Root Mean Square Error

where κ is the von Karman constant $(= 0.4)$, u^* is the friction velocity (in ms^{-2}) computed in (8), Ψ_h is the stability corrections for heat transport, L is the Monin–Obukhov length (in m), u_b is the wind speed measured at each of the three micrometeorological stations at the blending height z_b and 200 m and is assumed here (in ms^{-2}), z_d is the displacement height (in m), and z_{om} is the momentum roughness length (in m) estimated based on the exponential relationship between the reflectance of the NIR and red bands [14] as

$$z_{\mathrm{om}} = \exp\left(0.1021 + 0.1484(\rho_{\mathrm{NIR}}/\rho_{\mathrm{red}})\right). \tag{9}$$

Latent heat flux is then derived as the residual of the surface energy balance equation [i.e., via (2)].

B. Terrain Correction

Regional ET estimation often assumes a horizontal land surface such that the solar azimuth and solar elevation angles are constant over the area of interest at the satellite overpass time. In a mountainous watershed, however, these angles are different for each pixel depending on the slope and aspect. Shadow effects caused by mountains further cause variation in incoming solar radiation. Accurate ET estimations using satellite images in mountainous areas thus require that modifications, particularly terrain correction, be made to each pixel. Waters *et al.* [10] have recommended various modifications to improve the computation of components of the energy balance. In our proposed TSEBM module, terrain corrections are performed using topographic features extracted from two different DEMs (Fig. 2).

DEM_map and DEM_ASTER are first registered to the satellite images to ensure that all the data sets are within the same coordinate system. The registered DEMs and the VNIR and SWIR bands are then resampled into the same pixel size of their respective TIR bands. After resampling, the spatial resolution of Landsat-7 ETM+ associated data set is 60 m; that of ASTER is 90 m. Topographical features such as shaded relief and elevation are then extracted from the resampled DEMs using a topographical package in ENVI 4.6 and incorporated into respective equations of the incoming shortwave radiation $(K_s^{\downarrow})$, the atmospheric transmissivity (τ_{sw}), and the surface skin temperature (T_0) for terrain correction.

To correct the incoming shortwave radiation $(K_s^{\downarrow})$ in (3) for each pixel, solar azimuth angle, solar elevation angle, and shaded relief derived using DEM are incorporated as follows:

$$K_s^{\downarrow} = S_c \times R_{\mathrm{shade}} \times d_r \times \tau_{\mathrm{sw}} \tag{10}$$

where S_c is the solar constant (1367 Wm^{-2}), R_{shade} is the shaded relief (ranging from 0 to 1), d_r is the inverse squared relative Earth–Sun distance, and τ_{sw} is the atmospheric transmissivity.

In a mountainous terrain, the atmospheric transmissivity (τ_{sw}) varies for each pixel as a function of the elevation. The following equation from Allen *et al.* [15] is adopted for correction of the transmissivity as follows:

$$\tau_{\mathrm{sw}} = 0.75 + 2 \times 10^{-5}(E_{\mathrm{DEM}}) \tag{11}$$

where E_{DEM} is the elevation of each pixel.

As for surface skin temperature (T_0) used in (3) and (7), the rate of decrease in surface skin temperature due to elevation increase is assumed to be 0.65 °C/100 m, which is the same as that for a typical air profile [10]. The terrain correction for surface skin temperature is computed as

$$T_s = T_0 + 0.0065(E_{\mathrm{DEM}} - E_{\mathrm{ref}}) \tag{12}$$

where E_{ref} is the elevation of the micrometeorological station at which wind speed is measured.

IV. RESULTS AND DISCUSSION

A. Comparison of Surface Energy Flux Estimations

Surface heat fluxes are estimated using five models: the proposed TSEBM module with DEM_map, the proposed TSEBM module with DEM_ASTER, the Surface Energy Balance Algorithms for Land (SEBAL) Mountain model developed by the University of Idaho [10] with DEM_map, the SEBAL with DEM_ASTER, and the flat surface model based on the proposed TSEBM module without incorporating topography. The estimations from the five models are compared with the *in situ* measurements from the three micrometeorological stations (Table I). The results indicate that, for net radiation, sensible and latent heat fluxes, the correlation coefficients between the TSEBM with DEM_ASTER, and the *in situ* measurements are the highest among the five models. Also, the RMSEs for soil heat, sensible heat, and latent heat fluxes from the TSEBM with DEM_ASTER are lower than those from the flat surface model and the SEBAL Mountain model. Terrain correction incorporated in the proposed TSEBM module appears to be effective in increasing the estimation accuracy of surface heat fluxes in the study area.

For soil heat flux, however, the results exhibit low correlation coefficients between the *in situ* measurements and the model

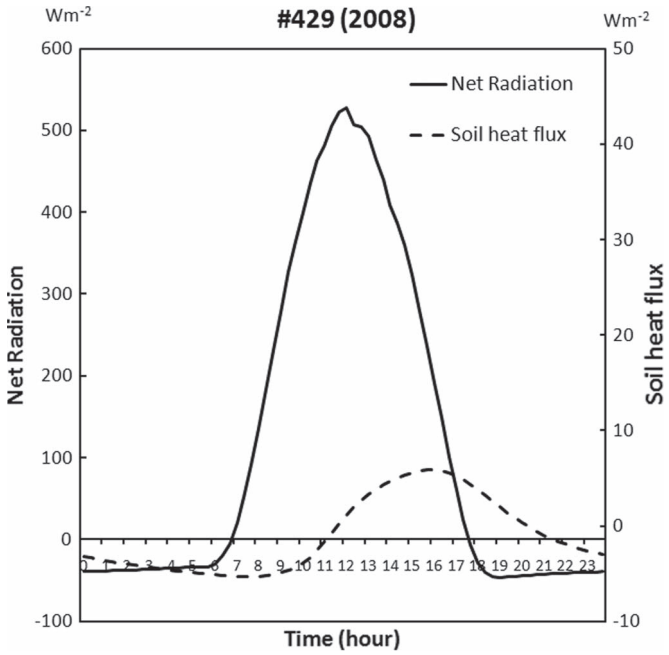

Fig. 3. Comparison between annual average net radiation and soil heat flux measured at the meteorological station (site #429) in 2008.

estimations, particularly those from the SEBAL and the TSEBM (Table I). Unlike the observation by Ogée *et al.* [16] suggesting a common time delay of 30 min between the maxima of net radiation and soil heat flux, our *in situ* measurements shows a delay of about 4 h (Fig. 3). It is probable that the soil heat flux in Mae Sa cannot be taken just as a fraction of the net radiation transmitted through the forest canopy, and the diurnal patterns of the energy fluxes could be incorporated into soil heat flux estimation for further improvement.

B. Comparison With the GVMI

Comparison of surface energy flux estimations suggests that the TSEBM module with DEM_ASTER estimates latent heat flux more accurately than the other four models. The TSEBM module with DEM_ASTER and (1) are thus employed over the entire Mae Sa watershed to derive regional ET distribution [Fig. 4(a)]. To examine if the spatial variation of ET in the watershed is associated with vegetation water content, the Global Vegetation Moisture Index (GVMI) proposed by Ceccato *et al.* [17] is calculated using the following equation:

$$GVMI = \frac{(NIR + 0.1) - (SWIR + 0.02)}{(NIR + 0.1) + (SWIR + 0.02)}. \tag{13}$$

The regional ET distribution is then compared with the GVMI (Fig. 4). The patterns of ET and GVMI are, in general, similar, particularly in the western part of the watershed. High ET is expected to be found on south-facing slopes, and high GVMI suggests dense forested areas. The central-northern area, which has south-facing slopes and is forested, appears to experience very high ET. The patterns of ET and GVMI in the central-south area are, however, dissimilar [comparison of Fig. 4(a) and (b)], suggesting that terrain and some other effects such as wind flow on ET may need to be considered.

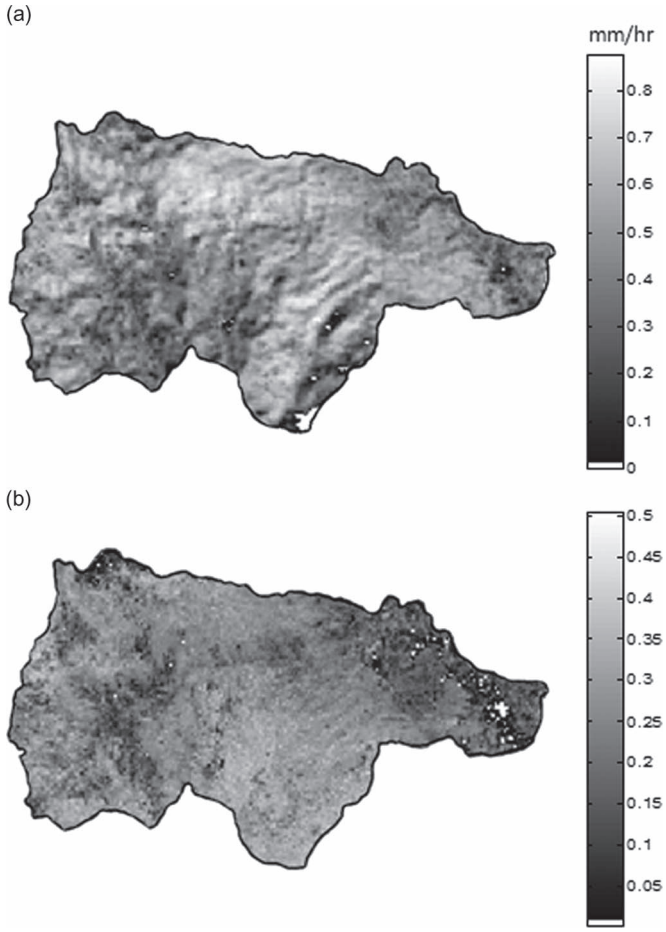

Fig. 4. Distributions of (a) ET and (b) GVMI derived using the ASTER image dated February 02, 2008. White areas corresponding to the zero value were caused by clouds in the original images.

V. CONCLUSION AND FUTURE WORK

In this letter, we have proposed a module that incorporates satellite images, surface meteorological data, and topographic information to estimate the ET in a mountainous watershed. Compared with the estimations derived from other models, our TSEBM module with terrain corrections using the ASTER DEM can increase the estimation accuracy of latent heat flux associated with ET, as evident in the highest correlation coefficient between the *in situ* measurement and the estimation ($R = 0.75$). The result indicates the usefulness of the TSEBM module in estimating spatially distributed ET over mountainous areas if the ASTER DEM can be acquired. Note that the scaling issue among various data sources needs to be further considered, but some assumptions have been made in this letter to minimize this problem. For example, when integrating the point meteorological data with satellite images and topographic information in (7)–(9), a blending height at 200 m was assumed so that the friction velocity could be estimated on a pixel-by-pixel basis. Future work could enhance the proposed module in two aspects. First, the estimations of surface energy fluxes, particularly in soil heat flux, can be further improved. Air flow and wind speed can be incorporated, although predicting the changes in the wind profile for each pixel in mountainous areas would be difficult. Second, despite the usefulness of the

ASTER DEM in the proposed module, some anomalous values in the DEM product may impede the analysis. An alternative approach is to employ the Moderate-resolution Imaging Spectroradiometer (MODIS) data that are low cost and high quantity. For example, the combination of Aqua and Terra satellites can provide up to four images per day, allowing the dynamics of surface energy fluxes to be monitored.

ACKNOWLEDGMENT

The authors would like to thank A. D. Ziegler and T. W. Giambelluca for providing *in situ* measurements through their National Aeronautics and Space Administration Grant NNG04GH59G, the Asia Pacific Network Grant ARCP2008-01CMY, and the NUS Grant R-109-000-092-133.

REFERENCES

[1] E. T. Engman and R. J. Gurney, *Remote Sensing in Hydrology*. London, U.K.: Chapman & Hall, 1991.

[2] L. Zhang, R. Lemeur, and J. P. Goutorbe, "A one-layer resistance model for estimating regional evapotranspiration using remote sensing data," *Agric. For. Meteorol.*, vol. 77, no. 3/4, pp. 241–261, Dec. 1995.

[3] J. C. Price, "Using spatial context in satellite data to infer regional scale evapotranspiration," *IEEE Trans. Geosci. Remote Sens.*, vol. 28, no. 5, pp. 940–948, Sep. 1990.

[4] J. Qin, S. Liang, R. Liu, H. Zhang, and B. Hu, "A weak-constraint-based data assimilation scheme for estimating surface turbulent fluxes," *IEEE Geosci. Remote Sens. Lett.*, vol. 4, no. 4, pp. 649–653, Oct. 2007.

[5] W. G. M. Bastiaanssen, M. Menenti, R. A. Feddes, and A. A. M. Holtslag, "A remote sensing surface energy balance algorithm for land (SEBAL). 1. Formulation," *J. Hydrol.*, vol. 212/213, pp. 198–212, Dec. 1998.

[6] E. Boegh, H. Soegaard, and A. Thomsen, "Evaluating evapotranspiration rates and surface conditions using Landsat TM to estimate atmospheric resistance and surface resistance," *Remote Sens. Environ.*, vol. 79, no. 2/3, pp. 329–343, Feb. 2002.

[7] M. Guardiola-Claramonte, P. A. Troch, A. D. Ziegler, T. W. Giambelluca, J. B. Vogler, and M. A. Nullet, "Local hydrologic effects of introducing non-native vegetation in a tropical catchment," *Ecohydrology*, vol. 1, no. 1, pp. 13–22, 2008.

[8] The Upland Program Project Database, Stuttgart, Germany: Univ. Hohenheim, May 8, 2008. [Online]. Available: https://www.uni-hohenheim.de/sfb564_db/data/climate.html

[9] N. J. Rosenberg, B. L. Blad, and S. B. Verma, *Microclimate: The Biological Environment*, 2nd ed. New York: Wiley, 1983.

[10] R. Waters, R. G. Allen, M. Tasumi, R. Trezza, and W. G. M. Bastiaanssen, *SEBAL: Surface Energy Balance Algorithms for Land*. Washington, DC: NASA EOSDIS, 2002.

[11] D. D. Baldocchi, D. R. Matt, B. A. Hutchinson, and R. T. McMillen, "Solar radiation within an oak—Hickory forest: An evaluation of the extinction coefficients for several radiation components during fully-leafed and leafless periods," *Agric. For. Meteorol.*, vol. 32, no. 3/4, pp. 307–322, Sep. 1984.

[12] K. Saito, S. Ogawa, M. Aihara, and K. Otowa, "Estimates of LAI for forest management in Okutama," in *Proc. 22nd ACRS*, 2001, vol. 1, pp. 600–605.

[13] J. A. Businger, J. C. Wyngaard, Y. Izumi, and E. F. Bradley, "Flux-profile relationships in the atmospheric surface layer," *J. Atmos. Sci.*, vol. 28, no. 2, pp. 181–189, Mar. 1971.

[14] A. Sarwar and R. Bill, "Estimation of surface heat fluxes in the Indus Basin using ASTER imagery," *Pak. J. Water Resour.*, vol. 7, no. 1, pp. 53–64, 2003.

[15] R. G. Allen, L. S. Pereira, D. Raes, and M. Smith, "Crop evapotranspiration guidelines for computing crop water requirements," FAO Irrigation and Drainage Paper No. 56, Rome, Italy: Food Agric. Org. United Nations, 1998.

[16] J. Ogée, E. Lamaud, Y. Brunet, P. Berbigier, and J. M. Bonnefond, "A long-term study of soil heat flux under a forest canopy," *Agric. For. Meteorol.*, vol. 106, no. 3, pp. 173–186, Feb. 2001.

[17] P. Ceccato, N. Gobron, S. Flasse, B. Pinty, and S. Tarantola, "Designing a spectral index to estimate vegetation water content from remote sensing data: Part 1: Theoretical approach," *Remote Sens. Environ.*, vol. 82, no. 2/3, pp. 188–197, Oct. 2002.